Extreme “Catapult” ruptures of the Çardak Fault in the 6 February 2023 Mw 7.6 earthquake in Türkiye

CENK YALTIRAK (yaltirak@itu.edu.tr)
Istanbul Technical University
UFUK TARI
Istanbul Technical University https://orcid.org/0000-0002-0722-1899
AYNUR DİKBAŞ
İstanbul University-Cerrahpaşa https://orcid.org/0000-0003-4614-9399
ORKAN ÖZCAN
Istanbul Technical University https://orcid.org/0000-0002-7485-6157
İREM ELİTEZ
Istanbul Technical University https://orcid.org/0000-0003-2267-2628

Article

Keywords:

Posted Date: August 19th, 2023

DOI: https://doi.org/10.21203/rs.3.rs-3199409/v1

Abstract

During a Mw 7.6 magnitude earthquake on the Çardak Fault, extreme sinistral displacements occurred along 10 segments representing a 98 km-long surface rupture. The length of the segments ranges between 3.5 and 23.0 km. The surface rupture of the earthquake extends along a narrow deformation zone that is at least 10 cm-wide in places. In the step-over zones of the segments, the coseismic slip is distributed on numerous echelon ruptures where ≥0.5 m of left-lateral displacement is measured in a 1.3 km-wide zone and occasionally becomes completely undetectable. The most important feature of this earthquake is the measured maximum left-lateral displacement along the 98 km-long surface rupture, making it one of the seven earthquakes in the literature with the most extreme displacement (10.0-12.6 m), considering the earthquake magnitudes and fault lengths observed during the instrumental period.

Introduction

On February 6, 2023, two devastating earthquakes with Mw 7.8 and Mw 7.6 were recorded at 04:17 and 13:29 in southeastern Turkey[1,2]. The latter earthquake caused a 98 km-long surface rupture on the Çardak Fault, an east-west trending, left-lateral intracontinental fault that extends at a 45° angle to the transform segment of the East Anatolian and Dead Sea faults in southeastern Turkey (Fig. 1a). Remarkably, the surface rupture did not follow a boundary visible in the morphology and did not follow the previously mapped fault trace, but ran across the tops or steep slopes of mountains and ridges (Fig. 1b). The Çardak Fault Earthquake resulted in the rupture zone formed over the thin snowpack causing a unique 98 km-long rupture pattern and displacements of 10.0-12.6 m on the fault, and this phenomenon is widely discussed in social media[3].

Extreme ruptures

Over the past 168 years, the largest lateral displacements have been measured on surface ruptures of thrust and strike-slip faults between 9.5 and 18.7 m. Prior to the instrumental period, an earthquake with Mw greater than 8.1 on the Wairarapa Fault in New Zealand in 1855 caused a maximum displacement of 18.7±1 m along a 145 km-long fault[4]. In the 1857 earthquake on the San Andreas Fault, a surface rupture more than 300 km-long occurred, and the maximum displacement was measured as 9.5 m and the magnitude of the earthquake was calculated as M 8.25[5]. In the early instrumental period, in 1931, a rupture of the Fu-Yun Fault occurred with the maximum displacement of 14.6 m along a 180 km-long rupture, and the magnitude of the earthquake was M 7.9[6]. In the Damxung Earthquake of 1951, which had a magnitude (M) 8.0, a 200 km-long surface rupture with a displacement of 12 m occurred[7]. In the 1957 Gobi-Altai Earthquake, a lateral displacement of 9 m was observed along a 236 km-long surface rupture[7]. Statistics of recorded earthquakes in the world in the modern instrumental period revealed a relationship between displacement, magnitude, and fault length[7,8]. In 2013, a 205 km-long surface rupture occurred as a result of M_w 7.7 earthquake in Baluchistan, Pakistan, and the maximum displacement was measured to be 11.4±1.3/2.1 m[9,10]. Most recently, in 2016, the Kaikoura Earthquake in

New Zealand (M 7.8) measured a maximum displacement of 11.8±0.3 m on surface rupture of approximately 83 km along the Kekerengu (onshore)-Needles (offshore) Fault[11].

Clearly, extreme displacements on faults with strike-slip could be mapped much more accurately by both remote sensing and field observations during earthquakes after 2013[9,10,11,12]. The earthquake on the Çardak Fault, the second of the two major earthquakes that occurred in Turkey on February 6, 2023, in the Kahramanmaraş-Elbistan region, occupies a new place among the seven earthquakes mentioned above with its extreme displacements.

Çardak Fault Earthquake Segmentation and surface rupture area

The Çardak Fault is a secondary fault conjugate to the Riedel P fractures, which make a 30° angle to the East Anatolian Fault Zone in an approximately counterclockwise direction (Fig. 1A). The surface rupture of the fault was traced in the field for 98 km between coordinates 38º00’09.38” N-36º30’19.86” E in the west and 37º58’17.72” N-37º36’10.10” E (Kuztepe) in the east (Fig. 1B). To the west, the surface rupture terminated to south of Göksun town. According to the displacements observed in the field, the surface rupture does not extend southwest as also observed in the aftershock distribution, but in a westerly direction toward the main road of Göksun town (https://atlas.harita.gov.tr/#14.41/37.99865/36.52425). According to field observations, it is clear that the rupture does not continue toward southwest or is not reflected on the surface according to the aftershock distribution (Fig. 1B). To the east, the surface rupture terminated at the edge of Kuztepe peak (KT), which is located south of Bıçakçı village (Figs. 1B and 1C). Even from this point, the surface rupture did not continue eastward. No lateral displacement was observed on either the Çığlık Fault, which ruptured during the earthquake, the Sürgü Fault, where limited aftershocks were recorded, or the Malatya Fault to the northeast (Fig. 1B, detailed observations available at https://atlas.harita.gov.tr/#9.85/38.001/37.1529).

Although the distribution of aftershocks following the major earthquakes suggest large-scale deformation, the rupture signature at the surface and our deformation measurements do not provide evidence for aftershocks on faults angled toward the Çardak Fault extent the rupture in those directions. These aftershocks showed oblique normal fault solutions angled toward the left-lateral Çardak Fault, dominated by a normal component in the northeast-southwest direction, whereas the left-lateral shear at the beginning and end of the fault has very few left-lateral components (Fig. 1B, Supplementary Table 3). The surface rupture caused by the last earthquake on the Çardak Fault resulted in 10 separate segments that step over each other. The length of these segments ranges from 3.5 to 23.0 km (Fig. 1C). Surface rupture on the Çardak Fault was observed predominantly within a narrow deformation zone of a few meters, and it was observed to occasionally split into branches within a few hundred meters of the step over (Supplementary Fig. 1, Table 1; Locality 69-77, 78-87, 92-97, 97-104, 108-109, 111-118, 119-127, 166-175, 216-218).

Extreme displacements on Çardak Fault and on-fault/near-fault displacement pattern.

Ten displacement measurements on the Çardak Fault are between 10 and 12.6 meters. In addition, displacements between 8 and 9.9 m were measured in 44 localities, between 5.0 and 7.9 m in 144 localities and between 0.1 and 49 m in 115 localities (Supplementary Table 1). Among them are five important sites from west to east (Figure 2). Of these sites, the largest left-lateral displacement was measured as 12.6 m at Korkmaz (Figure 2A-2A'). The other lateral displacements measured from west to east were 10.5 m at Uzunsırt (Figure 2B), 10.3 m at Kümeevleri (Figure 2C-2C'), 10.5 m at Doğu Barış (Figure 2D-2D'), and 12.3 m at Sarıdaş (Figure 2E-2E'), respectively. During the fieldwork, a newly constructed garden fence at Korkmaz locality was found to be displaced by the fault. Data were collected using a Real-Time Kinematic (RTK) integrated Unmanned Aerial Vehicle (UAV) at this location with an accuracy of one centimeter. Field measurements were compared to these data, which showed that the garden fences were offset as 12.6 and 11.0 meters, respectively. At the same time, to the west, displacements in this section of the fault decreased from 9.2 to 8.7 m in a distance of 200 m (Fig. 2A-2A'). In the Uzunsırt locality, the UAV-derived orthophotos showed that the road was displaced 10.5 m by the fault (Fig. 2B). In the Kümeevleri locality, a 10.5 m left-lateral offset was identified by measurements obtained by comparing pre- and post-earthquake orthophotos on a streambed and a road close to each other (Fig. 2C-2C'). One of the most remarkable extreme displacements measured east of Barış Village was determined by mapping building locations very close to the fault on pre- and post- earthquake orthophotos.

A farmhouse and its wall in the northern block moved 6.3 m to the west and a pool in the southern block moved 4.2 m to the east parallel to the fault, for a total relative movement of 10.5 m (Figure 2D-2D'). Similarly, a dirt field road in Sarıdaş region moved 8.6 m to the west in the northern block and 3.7 m to the east in the southern block, totaling 12.3 m (Figure 2E-2E').

In these observations, taking into account the data showing that buildings and fixed points located close to the fault on a block moved away from the fault in two different directions, the nature of the relative movement relationship between the pre- and post- earthquake points is shown on orthophotos, on the northern and southern blocks of the fault/fault zone in areas up to 500 m from the fault.

The relative motions of the selected points on the northern and southern blocks of the outer periphery were measured in a range between 10.0 and 11.8 m at 8 locations, 8.0 and 9.8 m at 21 locations, 5.3 and 7.8 m at 41 locations, and 0.4 and 4.9 m at 23 locations (Supplementary Table 2).

The two different sets of measurements made in this study have raised new and interesting questions. The most striking difference between the on-fault and near-fault observations is that the on-fault measurements sometimes exceed the near-fault measurements. When all displacements are graphed, it is noteworthy that there is a relationship between the on-fault and near-fault area that has never been recorded in earthquakes before (Figure 3). The second phenomenon is that observations along the fault

show a gradual decrease in displacement before large displacements occur, followed by a sudden and dramatic increase (Figure 3A). Observations along the fault show that there are eight different jump points towards the west. There are also eight examples of low-value displacements that gradually decrease towards the east (Figure 3A). Moreover, such sudden jumps are not common along the fault rupture (Figure 3B). A third phenomenon observed when comparing the two sets of displacement values is that the on-fault displacement exceeds the near-fault displacement at 20 sites (Figure 3C).

Discussion

The three new phenomena identified in this study contribute to the problems that have recently appeared in the literature concerning the nature of tearing[9,10,11,12].

These problems are;

1. The average of displacements at a zone boundary 500 m from the fault is 23% greater than the average of displacements on the fault. In general, displacements on the fault are expected to decrease with distance. This is contrary to the general findings in the literature.

2. It is observed that not only major but also minor on-fault displacements at twenty locations are higher than the near-fault displacements at twenty localities (Fig. 3C). Although this is consistent with the phenomenon that displacement on the fault decreases with distance in these sections, it exhibits a reverse pattern that is intertwined with the phenomenon in point 1 (Fig. 3C).

3. The extreme displacements occur suddenly, decrease over a short distance, and reappear during rupture at a higher rate than the displacements over a few hundred meters on either side of the movement. This raises the question of whether the exceptional displacements along the surface rupture are true displacements.

The literature search revealed that the earthquake on the Çardak Fault Earthquake is one of the seven extreme earthquakes where the kinematic limits were exceeded according to the relationships between maximum displacement and surface rupture length determined by Wells and Coppersmith[7]. However, when maximum displacement and magnitude are considered, a 98 km-long fault with a displacement of 12.6 m and a magnitude of Mw 7.6 is unusual (Fig 4). In this century, direct aftershock observations have extended the limits of measurements on the Kaikoura Fault[11]. The distribution of displacements on the fault that we measured appears to be unique. Our measurements associated with the earthquake on the Çardak Fault indicate that the average displacement measured within a 1-kilometer zone is greater than the average displacement measured on the fault. In this case, displacement accumulation on the fault may still occur. In the Baluchistan earthquake, geodetic methods were used to assess the complexity of the fault using satellite data[9,10,12]. In their study, the researchers used remote sensing for the first time to show the relationships in the displacement distribution on and near the fault with the advantage of unvegetated terrain.

In contrast to the extreme displacements in previous studies, the sawtooth-shaped structure of the Çardak Fault (Fig 3A), the sudden and extraordinary increase in displacement, the slowing of the barriers on the fault surface, and displacements that exceed the actual displacements like a bucket flying out of a catapult at the points where they are exceeded are new. In this case, we assume that the sudden displacement increases can continue to move on the ground with an extraordinarily fast motion as the fault progresses, because a near-surface section is freed from the obstacle as it is overcome due to the rock properties and geometry of the fault. In short, in this study, we define for the first time the phenomenon of a gradual decrease in displacement along a fault trace at the time of an earthquake and a sudden extraordinary increase in displacement as a sudden rupture effect, and we present this type of extreme motion for discussion as ***catapult rupture***. Another interesting feature of the Çardak Fault Earthquake is that the displacement disappears on the marble ridges and reappears in the valleys (Supplementary Fig. 1j). This indicates that the active fault connects old discontinuities at depth and that there are transitions indicating that it is a very young structure. At the surface, it is considered not to cut through the more rigid marble strata, but proceeds in the schists and mélange beneath these units. Analysis of the relationship between the displacements of the Çardak Fault and the rocks through which the fracture propagates, and comparison with the distribution of faults, could lead to a better understanding of these catapult ruptures and extreme displacements. Another remarkable observation is the variability of displacement over such short distances. This raises the question of whether previous studies with few directly measured observations in the field reflect the nature of faulting. For the first time, measurements before and after a surface rupture using high-resolution orthophotos and UAV measurements have led to the conclusion that previous methods are inadequate. Starting with the 2013 Balochistan[9,10,12] and 2016 Kaikoura earthquakes[11,13] and continuing with the 2023 Çardak Fault, research on the nature and measurement of faults using new technologies[14] raises new questions. High-resolution techniques such as UAVs, orthophotos and lidar data can now closely measure surface ruptures and their effects. Mapping seismic gaps by using pre-earthquake orthophotos and lidar images will usher in a new era of fault analysis.

Methodology and Data

In the days following the Çardak Fault Earthquake, 27x27 cm resolution orthophotos were collected by the General Directorate of Mapping (HGM) to determine the effects of the earthquake in the region. The photos were made available to the public on February 21, 2023, in the HGM Küre[15] mapping system. In addition, the orthophotos of the Çardak Fault taken between June 21, 2018 and September 30, 2020 were available as layers in the system. In this study, the surface rupture of the Çardak Fault was first mapped with the HGM Küre program at a resolution of 27 cm, and the displacements were listed (Fig. 1C; Supplementary Table 1). The surface rupture was identified and plotted on orthophotos, and the natural and artificial traces cut by the fault were listed. In addition, displacements parallel to the fault were measured between the positions of the natural and artificial points before and after the earthquake at distances up to 80 m away from the fault were also measured (Supplementary Table 1). For the orthophoto measurements on the error margin of ±27 cm thanks to the proximity of the comparison

points and the standard rectification of the orthophotos (Supplementary Table 1). In addition to the observations on- fault observations, considering the parallel boundaries established 500 m north and south of the fault/fault zone, displacements parallel to the main fault were measured between the before and after earthquake positions at natural and man-made fixed points close to these boundaries and listed as observations near fault (Supplementary Table 2). A field survey was conducted to verify the 227 measurement points. In this section, data obtained with a UAV and first stage data were verified by observation at points deemed necessary with a direct tape measure in the field. Depending on the flight altitude, digital surface models were created with 1-5 cm resolution. Measurement accuracy ranged from ±2-±8 cm. Direct measurements were added to 227 locations in Supplementary Table 1. On the orthophotos that form the basis of this study, 93 measurements were made near- fault and 311 on-fault measurements were made at points 500 m north and south of the main fault zone. During the field study, UAV measurements were made at 58 locations and direct field measurements were made at 35 locations.

Declarations

Acknowledgements

We would like to thank the GIS Department of the Ministry of Urbanization, Environment and Climate for providing the orthophotos used in this study, Rindan Community for providing financial and logistical support for the field work, Elbistan and Maraş Off-Road clubs for providing transportation with their off-road vehicles in the field, Istanbul Technical University Research Fund (MÇAP-2023-44519) for providing the necessary facilities to evaluate the data we collected in the study and ITU Rectorate for their contributions to this study.

Author information

Authors and Affiliations

1. İstanbul Technical University, Faculty of Mines, Department of Geological Engineering, 34467, İstanbul, Türkiye

Cenk Yaltırak, Ufuk Tarı, İrem Elitez

2. İstanbul University-Cerrahpaşa, Faculty of Engineering, Department of Geological Engineering, 34500, İstanbul, Türkiye

Aynur Dikbaş

3. İstanbul Technical University, Institute of Eurasian Earth Sciences, 34467, İstanbul, Türkiye

Orkan Özcan

Contributions

CY, He wrote the initial text of the manuscript, prepared the figures, took part in the calculation of the orthophoto measurements and the measurements in the field work. U.T. Produced DSM from UAV measurements in field surveys and documented tables for classification and supplementary of field surveys. A.D. She was involved in direct measurements in field work and displacement measurements of the DSMs produced from UAV data. O.Ö. Piloted the UAV in the field and participated in the processing of the collected data. İ.E. took part in direct measurements during field work. During the study, she performed identification of geological formations and measurements on the fault. U.T., A.D., O.Ö., İ.E. reviewed and edited the final text.

Corresponding author

Correspondence to Cenk Yaltırak

Ethics declarations

Competing interests

The authors declare no competing interests.

References

1. Melgar, D. et al. Sub- and super-shear ruptures during the 2023 M_w 7.8 and M_w 7.6 earthquake doublet in SE Türkiye. *Seismica* **2**, 1–10, https://seismica.library.mcgill.ca/article/view/387/521 (2023).
2. Goldberg, D. et al. Rapid Characterization of the February 2023 Kahramanmaraş, Türkiye, Earthquake Sequence. *The Seismic Record* **3**, 2, 156–167. https://doi.org/10.1785/0320230009 (2023).
3. https://twitter.com/CYaltirak/status/1632111872009818113?s=20 (March 04.2023)
4. Rodgers, D. W. and Little, T. A. World's largest coseismic strike-slip offset: The 1855 rupture of the Wairarapa Fault, New Zealand, and implications for displacement/length scaling of continental earthquakes, *J. Geophys. Res.,* **111**, B12408, http://doi:10.1029/2005JB004065 (2006).
5. Sieh, K. Slip along the San Andreas fault associated with the great 1857 earthquake, *Bull. Seismol Soc.Am.* **68**, 1421-1428, (1978).
6. Baljinnyam, I. et al. Ruptures of Major Earthquakes and Active Deformation in Mongolia and Its Surroundings. *Geological Society of America Memoir* **181,** 1-60 (1993).
7. Wells, D. L. and Coppersmith K. J. Empirical relationships among magnitude, rupture length, rupture area, and surface displacement, *Bull. Seismol. Soc. Am.*, 84, 974– 1002. (1994).
8. Wesnousky, S. G. Seismological and structural evolution of strike-slip faults. *Nature* **335,** 340–342, https://doi.org/10.1038/335340a0 (1988).
9. Zinke, R. Hollingsworth, J. and Dolan J. F. Surface slip and offfault deformation patterns in the 2013 MW 7.7 Balochistan, Pakistan earthquake: Implications for controls on the distribution of near-

surface coseismic slip, *Geochem. Geophys. Geosyst.* **15,** 5034–5050, http://doi:10.1002/2014GC005538 (2014).

10. Gold, R. D. et al. On-and off-fault deformation associated with the September 2013 M w 7.7 Balochistan earthquake: implications for geologic slip rate measurements, *Tectonophysics* **660,** 65-78. http://dx.doi.org/10.1016/j.tecto.2015.08.019 (2015).
11. Kearse, J. et al. Onshore to Offshore Ground-Surface and Seabed Rupture of the Jordan–Kekerengu–Needles Fault Network during the 2016 M_w 7.8 Kaikōura Earthquake, New Zealand. *Bulletin of the Seismological Society of America* **108** (3B), 1573–1595, https://doi.org/10.1785/0120170304 (2018).
12. Barnhart,W.D. et al Evidence for slip partitioning and bimodal slip behavior on a single fault: surface slip characteristics of the 2013 M_w7.7 Balochistan, Pakistan earthquake *Earth Planet. Sci. Lett.* **420.** 1-11. https://doi.org/10.1016/j.tecto.2015.08.019 (2015).
13. Little, T. A. et al. Kekerengu Fault, New Zealand: Timing and Size of Late Holocene Surface Ruptures. *Bull. Seismol. Soc. Am.* **108**, 1556–1572 https://doi.org/10.1785/0120170152 (2018).
14. Manighetti, I. et al. Repeated giant earthquakes on the Wairarapa fault, New Zealand, revealed by Lidar-based paleoseismology. *Sci Rep* **10**, 2124 https://doi.org/10.1038/s41598-020-59229-3 (2020).
15. https://kure.harita.gov.tr/

Figures

Figure 1

A: The region of Kahramanmaraş earthquakes and its location on Turkey, Çardak Fault location map. **EAFAS:** East Anatolian Fault Amanos Segment, **EAFPS:** East Anatolian Fault Pazarcık Segment, **ÇF:** Çardak Fault, **NF:** Narlı Fault, **CIF:** Çığlık Fault, **SF**: Sürgü Fault, **MF:** Malatya Fault. Coloured circles indicate locations of $M_w \geq 3$ earthquakes (https://deprem.afad.gov.tr/event-catalog). The topographic map was derived from the data produced by HGM with a resolution of 5 x 5 m, main faults were drawn on digital surface model (DSM). **B:** Fault plane solutions of $M_w \geq 4$ earthquakes on and around the Çardak Fault (Supplementary Table 3, https://deprem.afad.gov.tr/event-catalog), **C:** Surface rupture and segmentation along the Çardak Fault.

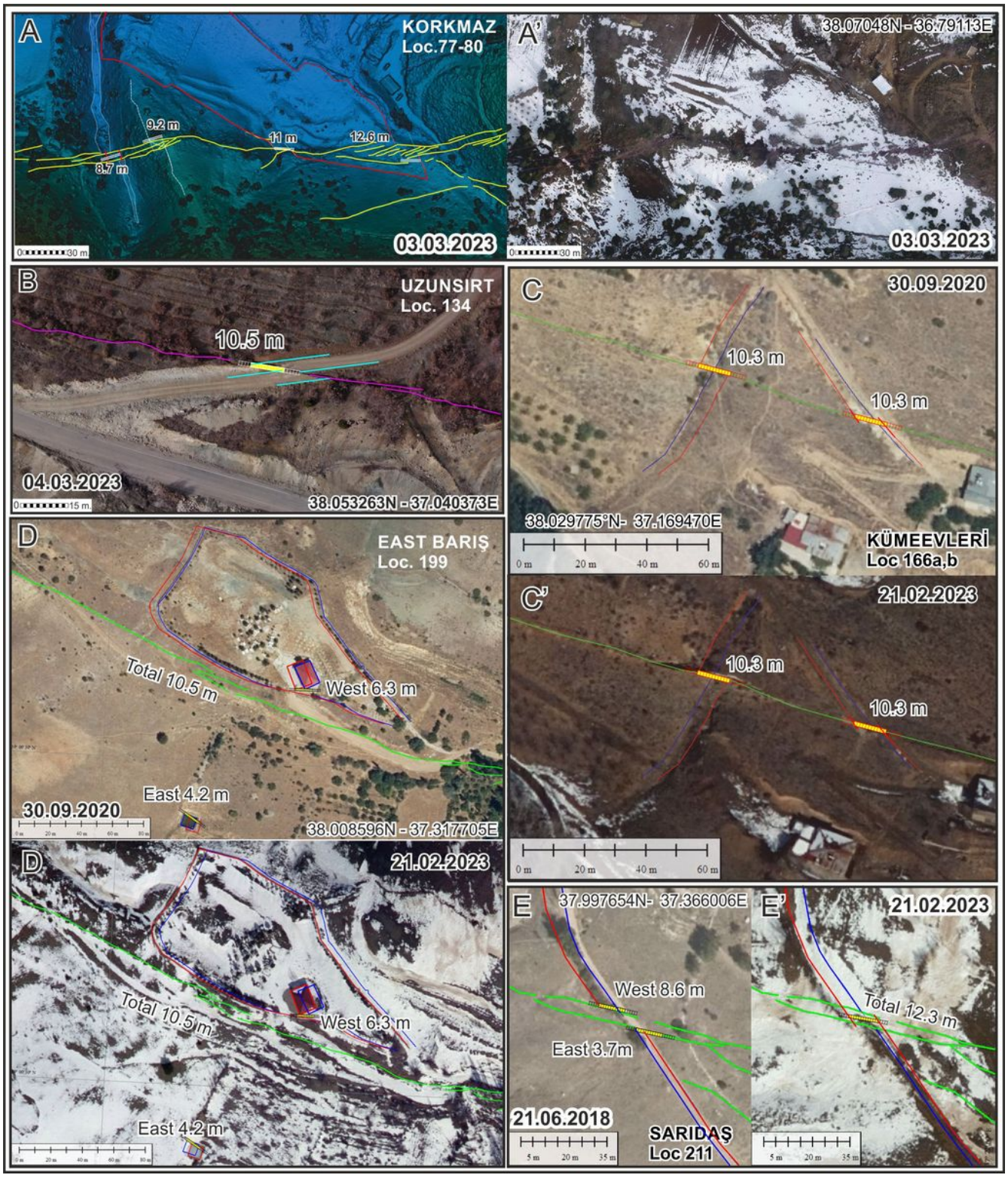

Figure 2

Examples of beats above 10 m from the study area. Dark blue lines represent pre-earthquake indicator, red lines represent post-earthquake indicator, green lines indicate surface rupture. **A:** Korkmaz UAV data, digital surface model **A':** Korkmaz UAV orthophoto, **B:** Uzunsırt UAV orthophoto, **C:** pre-earthquake orthophoto of Kümeevleri, **C':** post-earthquake orthophoto of Kümeevleri, **D:**pre-earthquake orthophoto of

eastern Barış Village, **D':** post-earthquake orthophoto of eastern Barış Village, **E:** pre-earthquake orthophoto of Sarıdaş, **E':** post-earthquake orthophoto of Sarıdas

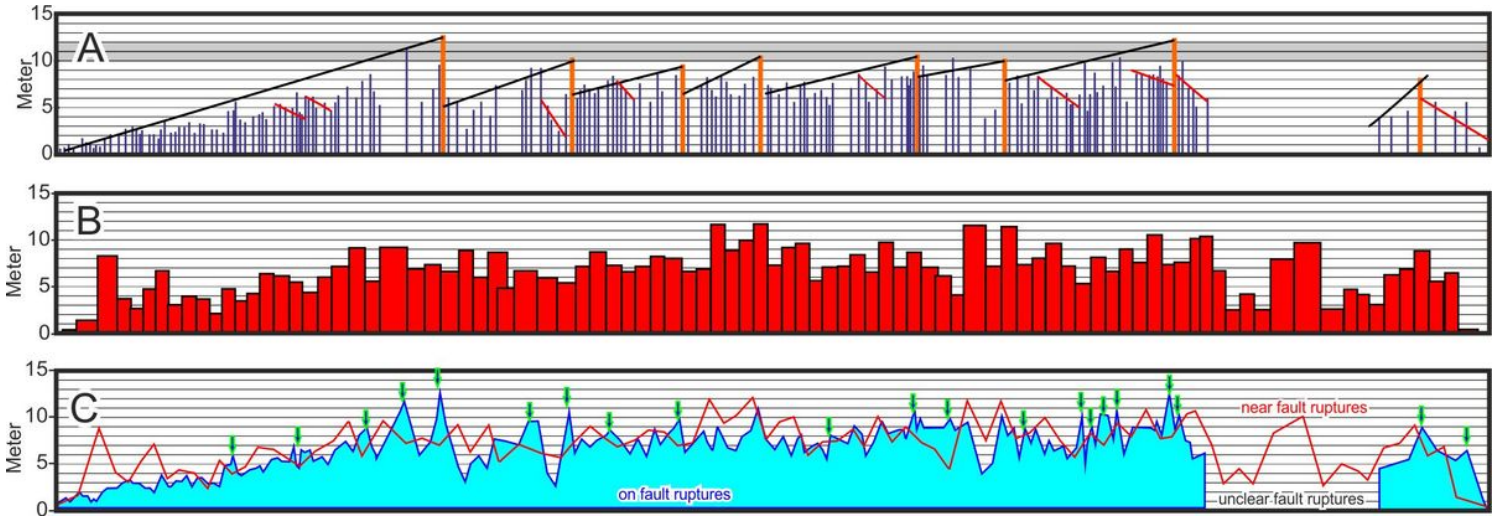

Figure 3

A: Distribution of on-fault measurements in the study area, the black lines sloping to the west show the decrease in translation after the Catapult rupture (orange lines), while the red lines show the minor reverse groups that increase to the west at lower displacement and decrease at the peak. **B:** Distribution of near-fault measurements in the study area, distribution of the amount of movement parallel to the fault with respect to each other at fixed points 500 m north and south of the fault. **C:**Comparison of on-fault and near-fault measurements. Green arrows indicate on-fault measurements exceedingly near-fault measurements.

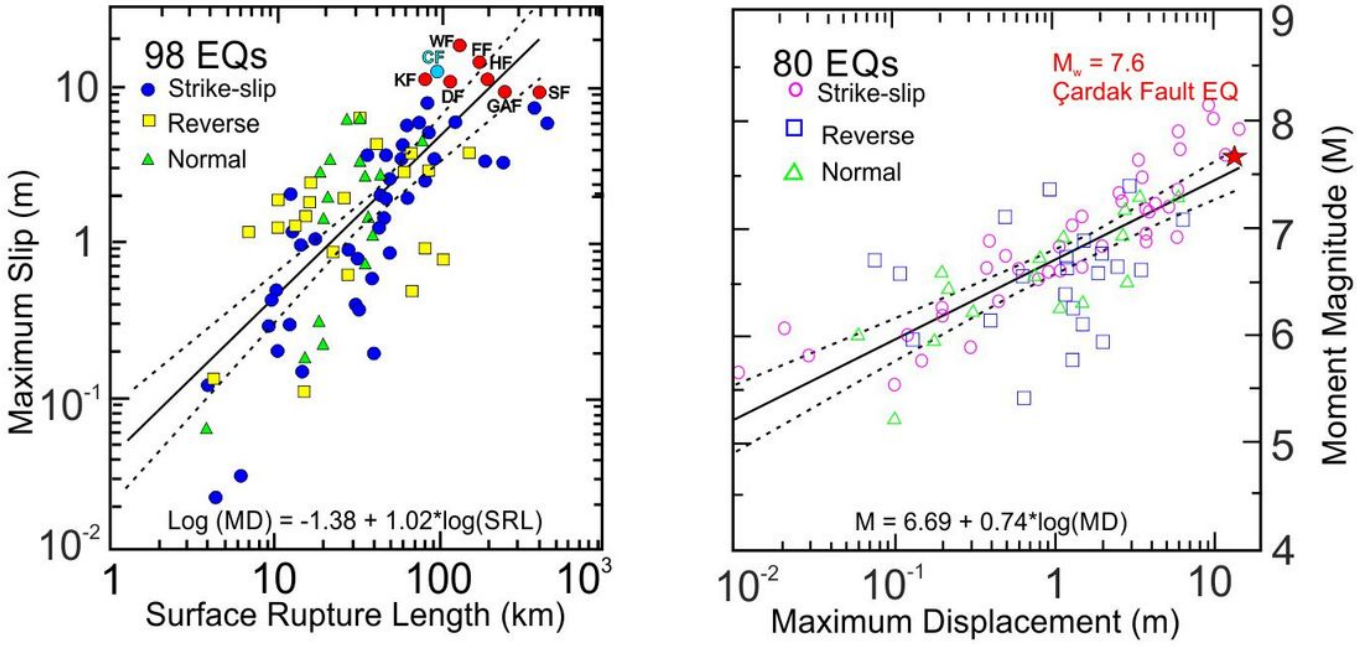

Figure 4

The graph on the left is revised by adding the position of the extreme displacements after year 2013 on the Maximum Slip/Surface rupture length defined by Wells and Coppersmith[7]. The faults of the extreme ruptures are WF: Wairarapa Fault, CF: Çardak Fault, KF: Kaikoura Fault, GAF: Gobi-Altai Fault. SF: San Andreas Fault, FF: Fu-yun Fault, DF: Damxung Fault, HF: Chaman Fault (Beluchistan). The graph on the right shows the position of the M_w 7.6 Çardak earthquake within the maximum displacement in the Maximum displacement/Moment Magnitude plot.

Supplementary Files

This is a list of supplementary files associated with this preprint. Click to download.

- SupplementaryYaltiraketalNatureComm.pdf